Domain C of Human Poly(ADP-ribose) Polymerase-1 Is Important for Enzyme Activity and Contains a Novel Zinc-Ribbon Motif[†,‡]

Zhihua Tao,[§] Peng Gao,[§] David W. Hoffman,*[,||] and Hung-wen Liu*[,§,||,⊥]

Division of Medicinal Chemistry, College of Pharmacy, Department of Chemistry and Biochemistry, and Institute for Cellular and Molecular Biology, University of Texas, Austin, Texas 78712

Received January 4, 2008; Revised Manuscript Received March 31, 2008

ABSTRACT: Poly(ADP-ribose) polymerase-1 (PARP-1) is a multimodular nuclear protein that participates in many fundamental cellular activities. Stimulated by binding to nicked DNA, PARP-1 catalyzes poly(ADP-ribosyl)ation of the acceptor proteins using NAD^+ as a substrate. In this work, NMR methods were used to determine the solution structure of human PARP-1 protein. Domain C was found to contain a zinc-binding motif of three antiparallel β-strands with four conserved cysteines positioned to coordinate the metal ligand, in addition to a helical region. The zinc-binding motif is structurally reminiscent of the "zinc-ribbon" fold, but with a novel spacing between the conserved cysteines ($CX_2CX_{12}CX_9C$). Domain C alone does not appear to bind to DNA. Interestingly, domain C is essential for PARP-1 activity, since a mixture containing nicked DNA and the PARP-1 ABDEF domains has only basal enzymatic activity, while the addition of domain C to the mixture initiated NAD^+ hydrolysis and the formation of poly(ADP-ribose), as detected by an NMR-based assay and autoradiography. The structural model for domain C in solution provides an important framework for further studies aimed at improving our understanding of how the various domains within the complex PARP-1 enzyme play their respective roles in regulating the enzyme activity when cells are under conditions of genotoxic stress.

Poly(ADP-ribose) polymerase-1 (PARP-1)[1] is an abundant nuclear protein that plays pivotal roles in many fundamental biological processes, including DNA repair, cell cycle regulation, gene expression, and cell death (*1*–*6*). It catalyzes the cleavage of NAD^+ into nicotinamide and ADP-ribose, the latter of which may be covalently attached to nuclear acceptor proteins as a branched polymer of poly(ADP-ribose), or PAR (Figure 1A). The enzymatic activity of

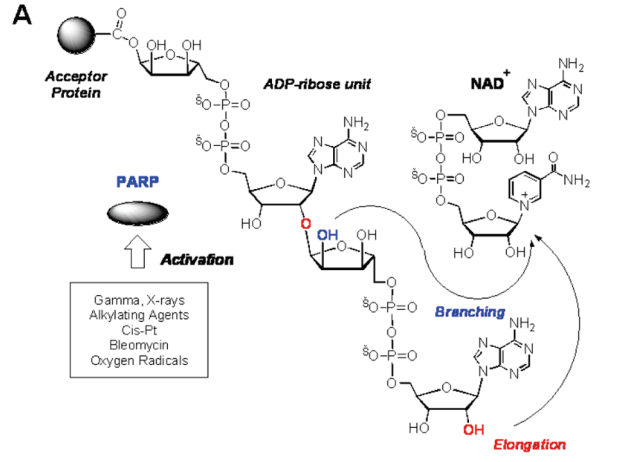

FIGURE 1: Schematic diagram of the reaction catalyzed by PARP-1 and the modular organization of PARP-1. (A) Synthesis of poly(ADP-ribose) from NAD^+ catalyzed by PARP-1. (B) Schematic representation of the domain structure of human PARP-1, showing the relative sizes and locations of domains A−F, and a nuclear localization sequence (NLS). FI and FII refer to the two previously identified zinc-finger motifs. Domain C has traditionally been included as part of the DNA binding domain, although there is no evidence that domain C by itself binds DNA.

[†] This work was supported by Grants F-1353 (to D.W.H.) and F-1511 (to H.-w.L.) from the Welch Foundation.

[‡] The coordinates for the structure of PARP-1 domain C have been deposited in the BioMagResBank with accession number 15602 and the Protein Data Bank as entry 2jvn.

* To whom correspondence should be addressed. H.-w.L.: phone, (512) 232-7811; fax, (512) 471-2746; e-mail, h.w.liu@mail.utexas.edu. D.W.H.: phone, (512) 471-7859; fax, (512) 471-8696; e-mail, dhoffman@mail.utexas.edu.

[§] Institute for Cellular and Molecular Biology.

[||] Department of Chemistry and Biochemistry.

[⊥] Division of Medicinal Chemistry, College of Pharmacy.

[1] Abbreviations: BRCA1, breast cancer susceptibility gene 1; BRCT, BRCA1 C-terminal motif; BSA, bovine serum albumin; CNS, crystallography and NMR system; DQF-COSY, double-quantum-filtered correlation spectroscopy; DSS, 2,2-dimethyl-2-silapentane-5-sulfonate; DTT, dithiothreitol; ELISA, enzyme-linked immunosorbent assay; FPLC, fast protein liquid chromatography; HCCH, $^1H-^{13}C-^{13}C-^1H$ multidimensional correlation spectroscopy; HEPES, 4-(2-hydroxyethyl)-1-piperazineethanesulfonic acid; HSQC, heteronuclear single-quantum coherence spectroscopy [HNCA, HNCACB, HNCO, HN(CO)CACB, and HACACBCO all refer to NMR pulse sequence programs]; ICP-MS, inductively coupled plasma mass spectrometry; IPTG, isopropyl β-D-thiogalactoside; LB, Luria-Bertani; LMCT, ligand to metal charge transfer; NAD^+, nicotinamide adenine dinucleotide (oxidized form); NLS, nuclear localization signal; NMR, nuclear magnetic resonance; NOE, nuclear Overhauser effect; NOESY, nuclear Overhauser spectroscopy; PAGE, polyacrylamide gel electrophoresis; PAR, poly(ADP-ribose); PARP-1, poly(ADP-ribose) polymerase-1; PBS, phosphate-buffered saline; PBST, PBS containing 0.1% (v/v) Tween 20; rmsd, root-mean-square deviation; SDS, sodium dodecyl sulfate; TEV, tobacco etch virus; TOCSY, total correlation spectroscopy.

10.1021/bi800018a CCC: $40.75
Published on Web 05/02/2008

PARP-1 is strictly dependent on the presence of interruptions in the DNA. It was shown that DNA strand breaks can stimulate the PARP-1 activity up to 500-fold over its basal level (*7*). With a low or moderate level of DNA damage, the attachment of PAR to acceptor proteins triggers the recruitment of repair enzymes to the damage sites, facilitating the base excision repair of DNA and cell survival. If the cell fails to repair the damaged DNA, caspase-3 will be activated and cleaves PARP-1 into two inactive fragments, which is one of the key events in apoptosis (*8*). In the case of more extensive DNA damage, overactivation of PARP-1 will cause the depletion of cellular energy pools, eventually leading to necrotic cell death (*9*). Under physiological conditions without DNA strand breaks, the basal activity of PARP-1 is required at sites of massive transcriptional activation such as puffs and nucleolus to promote expression of certain genes (*10, 11*).

PARP-1 is the first characterized and most extensively studied member of a superfamily of PARP proteins, related by their similarity in primary sequence (*12*). Early work from Shizuta's laboratory demonstrated that PARP-1 can be divided into three functional domains by limited proteolysis of the enzyme with papain and/or α-chymotrypsin: a 46 kDa N-terminal DNA binding domain, a 22 kDa centrally located automodification domain, and a 54 kDa C-terminal catalytic domain (*13*). The organization of PARP-1 has more recently been dissected into six smaller regions [domains A−F (Figure 1B)] based on homology with previously identified functional modules (*14*). Together, domains A and B are composed of two unique zinc-finger motifs ($CX_2CX_{28,30}HX_2C$) and a bipartite nuclear localization signal (NLS) and are sufficient to direct specific binding of the whole PARP-1 to the target damaged DNA (*15, 16*). The PARP-1 zinc fingers are structurally and functionally unique compared with the classical zinc fingers, due to the long length of the fingers and their recognition of altered DNA structures rather than specific DNA sequence (*15*). Domain D, corresponding to the automodification domain in the three-domain naming system, contains a BRCT motif which is likely an interface for PARP-1 to interact with other proteins (*17*). Domain E contains a WGR motif, which is defined by the conserved Trp, Gly, and Arg residues. The function of this domain remains uncertain, although Semighini et al. (*18*) has speculated that it is a possible nucleic acid binding region. Domain F is termed the minimal catalytic domain and is responsible for the basal DNA-independent catalytic activity (*19*). It possesses all three catalytic activities (initiation, elongation, and branching of PAR) associated with the full-length enzyme, as shown in Figure 1A. In human PARP-1, residues 859−908 within domain F are phylogenetically well conserved and are considered to be the "PARP signature" that unites the PARP family members (*14*).

Domain C, the subject of this work, appears exclusively in PARP-1; there is no homologous region in other PARP isoforms such as PARP-2 or centrosomal PARP-3, or in the tankyrases. Domain C does not appear to be significantly similar in primary sequence to any protein domain of previously known structure. It was predicted earlier that domain C contains two helix−turn−helix motifs, structural elements capable of DNA binding, at residues 200−220 and 280−285, suggesting that the contribution of domain C could be in recognition and binding of DNA (*20, 21*). Moreover, footprinting experiments have shown that a polypeptide consisting of domain C and domain D binds strongly to DNA and has a binding pattern similar to that of full-length PARP-1 (*22*). Arguing against this, Trucco et al. (*23*) using random mutagenesis screening identified two PARP-1 loss-of-function mutants, with the mutation sites located in domain C (K249E and G313E), that retain their full DNA binding capacity (*23*). This observation suggests that domain C might have roles in PARP-1 activity other than protein−DNA interactions. Clearly, the exact function of domain C in PARP-1 activation remains to be determined.

Detailed structural information in solution as well as in the crystalline state is essential in understanding the apparently complex regulatory mechanism of the PARP-1 enzyme and will provide valuable information that may eventually lead to the design of more potent and selective inhibitors. The detailed structure of PARP-1 is of particular interest, since the enzyme is involved in the regulation of cell death and its inhibitors are of great interest for cancer therapy. The solution structures of domains D and E [PDB entry 2cok for domain D and PDB entry 2cr9 for domain E (unpublished)], and the two individual zinc fingers in domain A [PDB entry 2dmj for zinc finger I and PDB entry 2cs2 for zinc finger II (unpublished)] from human PARP-1 have been determined by NMR methods. The structure of the catalytic F domain of PARP-1 has been determined by X-ray crystallography, by itself and in complex with inhibitors (*24, 25*). In this work, we focus on domain C and use NMR spectroscopy as the approach for structure determination, given the modest size of the protein. Complementing the structural results, the requirement of the presence of domain C for PARP-1 activity was demonstrated by comparing the PARP-1 activities of isolated domains ABDEF with and without domain C. Our studies suggest that domain C plays an important role in the architecture of catalytically active PARP-1. It is important to note that the crystal structure of a dimeric form of domain C was recently reported (*26*).

MATERIALS AND METHODS

Cloning, Expression, and Purification of Domain C. DNA encoding residues 233−373 of the human PARP-1 protein (termed domain C) was cloned into a maltose binding protein (MBP) fusion vector (MalE-pET) constructed in our laboratory at the *Nde*I and *Xho*I restriction sites. MalE-pET, a modified pET-24b(+) expression vector (Novagen), was designed so that domain C is expressed as a fusion protein with a polyhistidine-tagged MBP (His_{10}MBP) at the N-terminus, separated by a TEV protease cleavage site. The plasmid was transformed into *Escherichia coli* BL21-CodonPlus(DE3)-RP (Stratagene). Cells were typically grown at 37 °C in 6 L of LB broth containing kanamycin (50 μg/mL) and chloramphenicol (35 μg/mL) until the OD_{600} reached 0.5. Expression of the recombinant His_{10}MBP−domain C fusion protein was induced via the addition of IPTG to a final concentration of 0.2 mM. Cells were then grown for an additional 24 h at 18 °C, harvested by centrifugation, and stored at −80 °C. Thawed cells were resuspended in the lysis buffer [20 mM HEPES buffer (pH 7.5), 300 mM NaCl, 10 mM imidazole, 10% glycerol, and 1 mM β-mercaptoethanol] and sonicated to rupture the cell membrane. After centrifugation for 30 min at 18000*g* to

remove the cell debris, the supernatant was incubated with 10 mL of Ni-NTA agarose resin (Qiagen) for 1 h at 4 °C. Lysate and resin were then loaded onto a column, which was allowed to drain, and then washed with lysis buffer. The His_{10}MBP−domain C fusion protein was eluted from the column with the HEPES buffer described above containing 0.25 M imidazole. The desired protein fractions were pooled and dialyzed against the dialysis buffer (the components are the same as lysis buffer), and 2% (w/w) His_6-tagged TEV protease was added into the dialysis bag to cleave the His_{10}MBP. The unwanted His_{10}MBP and His_6TEV protease were removed by slowly filtering the mixture through a column of 10 mL of Ni-NTA resin, and the flow-through that contained nontagged domain C was then concentrated to 10 mg/mL by ultrafiltration on an Amicon concentrator using a YM 10 membrane (Millipore). Domain C was further purified by size exclusion chromatography using a Superdex 200 column (GE Healthcare) mounted on an AKTA FPLC system. During this step, the buffer was changed to 10 mM sodium phosphate buffer (pH 6.0) and 250 mM NaCl. Fractions containing domain C were identified by SDS−PAGE, pooled, and concentrated. The typical yield was 20 mg of purified domain C per liter of cell culture. Samples of domain C enriched in ^{15}N and/or ^{13}C were prepared following analogous procedures, but using M9 minimal medium containing [^{15}N]NH_4Cl (0.6 g/L) and/or [U-^{13}C]glucose (2 g/L) (Cambridge Isotope Laboratories) as the source of nitrogen and/or carbon when the cells were grown. Trace metals were added to the minimal medium as follows (per liter): 12 μg of $CuSO_4 \cdot 5H_2O$, 7.4 μg of $MnCl_2 \cdot 4H_2O$, 1.4 μg of $CoCl_2 \cdot 6H_2O$, and 3 mg of $ZnSO_4 \cdot 7H_2O$. The metal content of the purified protein was determined by ICP-MS at the Department of Geological Sciences, University of Texas.

Cloning, Expression, and Purification of Domains ABDEF. Genes encoding domains ABDEF (as a single polypeptide) were introduced into pET-28b(+) (Novagen) by deletion mutagenesis (*27*) using PARP-1/pET-28b(+) as the template and PG2 (5′-*GAA,AAA,GAC,AAG,GAT,AGT*,GAT,ATC,GCC,TCG,GCT,CCT,GCT,G-3′) and PG3 (5′-CAG,CAG,GAG,CCG,AGG,CGA,TAT,C*AC,TAT,CCT,TGT,CTT,TTT,C*-3′) as the primers, which contain the sequences of the 3′-terminus of PARP-1 domain B (italic) and the 5′-terminus of domain D (regular font) at each side. The resulting ABDEF/pET-28b(+) construct was digested with *Nde*I and *Xho*I, and the fragment encoding ABDEF was subcloned into the MalE-pET vector to give the recombinant ABDEF/MalE-pET plasmid. The expression and purification of ABDEF were carried out under the same conditions used for domain C, with the purified protein stored in dialysis buffer mentioned above.

NMR Spectroscopy. Samples used for determination of the structure of PARP-1 domain C contained 10 mM sodium phosphate buffer (pH 6.0), 250 mM NaCl, 1 mM sodium azide, a 90% H_2O/10% D_2O mixture or 99.9% D_2O, and typically 1 mM protein. Spectra were recorded at 25−35 °C using a 500 MHz Varian Inova spectrometer equipped with a triple-resonance probe and *z*-axis pulsed field gradient. Backbone resonance assignments were obtained using three-dimensional HNCA, HNCACB, HNCO, HN(CO)CACB, and HACACBCO spectra (*28*–*30*). Unambiguous backbone resonance assignments were obtained for residues 233−373, with the exception of four of the prolines. Resonance assignments for nearly all side chains were obtained by analyzing three-dimensional (3D) ^{15}N-resolved TOCSY-HSQC and ^{13}C-resolved HCCH-TOCSY (*31*) spectra, and two-dimensional (2D) homonuclear DQF-COSY and TOCSY spectra. NOE cross-peaks were detected using two-dimensional $^1H-^1H$ NOESY, three-dimensional $^1H-^1H-^{15}N$ NOESY-HSQC, and three-dimensional $^1H-^1H-^{13}C$ NOESY-HSQC with NOE mixing times of 60−120 ms. Although the spectra were acquired using a rather ordinary (500 MHz) field, the three-dimensional NOE spectra were acquired using a relatively high digital resolution, with a total acquisition time of 4 days for each spectrum. In addition, the ^{13}C- and ^{15}N-resolved three-dimensional NOE spectra were each acquired at two temperatures (25 and 35 °C) so that small chemical shift differences could be exploited to remove ambiguities in assigning NOE cross-peaks to specific pairs of protons and thus maximize the number of useable NOE restraints. A two-dimensional NOE spectrum acquired using a nonsaturating (jump−return) water suppression method was useful in obtaining NOEs for protons with relatively rapid rates of exchange with solvent, such as the hydroxyl proton of a threonine side chain in the zinc-binding domain. Data were processed using NMR-Pipe (*32*). Spectra recorded in 99.9% D_2O were useful in identifying amide protons that were involved in hydrogen bonds and protected from solvent exchange. Proton chemical shifts were measured relative to internal 2,2-dimethyl-2-silapentane-5-sulfonate (DSS) at 0 ppm. The ^{13}C and ^{15}N reference frequencies were determined by multiplying the 0 ppm ^1H reference frequency by 0.251449530 and 0.101329118, respectively (*33*). Chemical shifts were submitted to the BioMagResBank with accession number 15602.

Structure Calculation. The restrained simulated annealing protocol within CNS version 1.1 (*34*) was used to identify the structures that are consistent with the distance and angle restraints derived from the NMR data while having reasonable molecular geometry, and with a minimum value of the CNS energy function. Distance restraints were derived from the intensities of cross-peaks within homonuclear 2D NOE and ^{15}N-resolved and ^{13}C-resolved 3D NOE spectra obtained with relatively short mixing times of 60 ms to minimize the effects of spin diffusion. On the basis of the cross-peak intensity in the 60 ms NOE spectra, distance restraints were classified as strong (<3.2 Å), medium (<3.6 Å), weak (<4.0 Å), and very weak (<5.0 Å); these distance bounds were calibrated by using interproton distances in regions of regular secondary structure as internal distance standards. Additional cross-peaks observed in NOE spectra with mixing times of up to 120 ms were assigned to distance restraints as strong (<4.0 Å), medium (<5.0 Å), weak (<5.5 Å), and very weak (<6.0 Å). Pseudoatom corrections were applied to the distance restraints as follows. Distance restraints for valine or leucine methyl groups that were not stereospecifically assigned were measured from the center of the two methyl groups, and 2.4 Å was added to the interproton distance. For NOEs involving other methyl protons, distances were measured from the center of the methyl group and an additional 1.0 Å was added to the interproton distance. For NOEs involving methylene protons with no stereospecific assignment, distances were measured from the center of the methylene group and 0.7 Å was added to the interproton

Table 1: Summary of Refinement and Structural Statistics Obtained for Domain C of Human PARP-1[a]

no. of intraresidue NOEs	336
no. of sequential NOEs (residue i to $i + 1$)	537
no. of medium-range NOEs (residue i to $i + 2$, 3, or 4)	484
no. of long-range NOEs	318
no. of dihederal angle restraints (φ plus ψ)	224
no. of hydrogen bond restraints	53
total no. of structural restraints	1952
rmsd for residues 233−357, backbone atoms only	1.52 Å
rmsd for residues 233−357, all non-hydrogen atoms	2.77 Å
rmsd for residues 233−357, omitting residues 335−349, backbone atoms only	1.12 Å
rmsd for residues 233−357, omitting residues 335−349, all non-hydrogen atoms	2.36 Å
rmsd for zinc-binding motif, residues 291−332, backbone atoms only	0.49 Å
rmsd for zinc-binding motif, residues 291−332, all non-hydrogen atoms	1.44 Å
average no. of NOE violations >0.3 Å (per structure)	17.3
average no. of NOE violations >0.6 Å (per structure)	0
residues in the most favored regions of the Ramachandran plot	80.9%
residues in the additional allowed regions of the Ramachandran plot	18.3%
residues in generously allowed regions of the Ramachandran plot	0.9%
residues in disallowed regions of the Ramachandran plot	0.0%
rmsd for covalent bonds	0.011
rmsd for covalent angles	1.5

[a] Statistics were derived from a set of 16 structures, obtained by simulated annealing. Each structure was derived from a unique starting model and has a similar low value of the CNS ((*34*)) energy function.

distance. For NOEs involving δ and ϵ protons of tyrosine and phenylalanine rings, distances were measured from the center of the two δ or ϵ protons, and 2.4 Å was added to the interproton distance. Backbone dihedral φ and ψ torsion angle restraints for residues within regions of regular structure were derived from ^{13}C, ^{15}N, and ^{1}H chemical shifts using PREDITOR (*35*). Hydrogen bonds were included as distance restraints for residues within the regular α-helices and the antiparallel β-strands. Target values for the Zn−S bond lengths and Zn−S−C_β bond angles for residues 295, 298, 311, and 321 were 2.28 Å and 110°, respectively. Experimental restraints and structural statistics for domain C of human PARP-1 are summarized in Table 1.

An initial set of 20 diverse structures was generated from an extended peptide conformation using the CNS simulated annealing protocol, with dihedral angle restraints only. Each member of this set was then used to generate at least 10 structures each, via restrained simulated annealing, subject to angle and NMR-derived distance restraints, using different initial trajectories. A set of 16 refined conformers, each originating from a different starting structure and having the minimum value of the CNS energy function, was retained (Figure 4A), with statistics reported in Table 1. This final set of structures provides a fair representation of the full range that is consistent with the experimental data while having reasonable molecular geometry, with no NOE-derived distance restraint violations greater than 0.3 Å. The final set of PARP-1 domain C structures was deposited in the Protein Data Bank as entry 2jvn.

PARP-1 Activity Assays. The abilities of different mixtures of PARP-1 domains (ABDEF and ABDEF/C) to hydrolyze NAD^+ were examined by ^{1}H NMR spectroscopy. The reaction mixture having a final volume of 600 μL contained 10 μM ABDEF domains, 15 μM nicked DNA, and 10 mM $MgCl_2$ in NMR buffer, with or without 20 μM domain C. The reaction was initiated by the addition of 1 mM NAD^+. After gentle mixing, a total of 240 ^{1}H NMR spectra were recorded at 1 min intervals at 25 °C. The appearance of free nicotinamide and the consumption of NAD^+ were monitored by observing peaks in the ^{1}H NMR spectra corresponding to each species.

Poly(ADP-ribosyl)ation assays were also carried out using samples containing 1 μM ABDEF domains, with or without 5 μM domain C, incubated for 15 min at room temperature in 25 μL of assay buffer consisting of 100 mM Tris-HCl (pH 7.0), 10 mM $MgCl_2$, 5 μM NAD^+, 0.2 μCi of [α-^{32}P]NAD^+, and 5 μM nicked DNA. The reaction was terminated by the addition of an equal volume of 2× SDS loading buffer, and the samples were separated using a 12% SDS−polyacrylamide gel. The autopoly(ADP-ribosyl)ation was detected by the incorporation of [α-^{32}P]NAD^+ using a PhosphorImager (Molecular Dynamics).

Preparation of the DNA Ligand for NMR Titration. Single-strand 18-mer DNA (5′-GCATTCCTGCAGGAATGC-3′) and 44-mer DNA (5′-CGGTCGATCGTAAGATCGACCG-GCGCTGGAGCTTGCTCCAGCGC-3′) were obtained from IDT DNA Co. To prepare the double-strand 18-mer DNA and 44-mer nicked dumbbell DNA, the oligos were dissolved into annealing buffer [10 mM Tris-HCl buffer (pH 7.5) and 100 mM NaCl], heated to 95 °C for 4 min, cooled slowly to 4 °C, and then dialyzed in the same buffer as the protein sample discussed above. Domain C−DNA samples were prepared by slow addition of 100 or 250 μL of 0.75 mM ^{15}N-labeled domain C to 500 μL of 0.75 mM 18-mer double-strand DNA or 44-mer nicked dumbbell DNA. The resulting samples contain protein:DNA molar ratios of 1:5 or 1:2. Following each addition, a ^{1}H one-dimensional NMR spectrum was recorded. A $^{15}N-^{1}H$ correlated 2D NMR spectrum was also collected for the sample containing a 1:2 molar ratio of protein to nicked dumbbell DNA.

Dot Blotting Assay. The calf thymus DNA (Sigma) was covalently labeled using EZ-Link Photoactivatable Biotin (Pierce), following the manufacturer's protocol. For the dot blotting assay, 1 μL of a 1 mg/mL sample of domain C was first blotted onto a nitrocellulose membrane. The membrane was blocked with 50 mL of PBST [137 mM NaCl, 2.7 mM KCl, 1.5 mM KH_2PO_4, 8 mM Na_2HPO_4 (pH 7.4), 0.1% (v/v) Tween 20, and 5% (w/v) nonfat milk] at room temperature for 2 h. The membrane was then washed with 50 mL of PBS buffer [137 mM NaCl, 2.7 mM KCl, 1.5 mM KH_2PO_4, and 8 mM Na_2HPO_4 (pH 7.4)] and preincubated with 50 mL of DNA probe dilution buffer (0.3% BSA and 1% goat serum in PBS) for 1 h. The biotinylated calf thymus DNA was added to the probe dilution buffer to a final concentration of 10 μg/mL and incubated with the membrane at room temperature for 2 h. After four washes with PBS buffer, the formation of the domain C−DNA complex was detected by incubating the membrane with streptavidin-bound horseradish peroxidase (Pierce) for 30 min and washing it four times as described previously, and the signal was visualized using the Pierce chemiluminescence detection system.

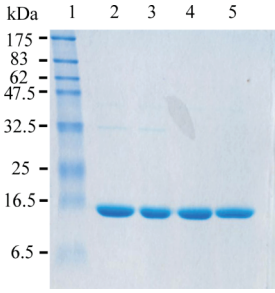

FIGURE 2: SDS−-PAGE gel (15%) of purified PARP-1 domain C: lane 1, molecular mass standards; lanes 2−5, purified domain C protein.

RESULTS

Overall Structure of Domain C. Domain C of human PARP-1, corresponding to residues 233−373, was overexpressed in *E. coli* and purified to homogeneity as determined by SDS−PAGE analysis (Figure 2). The domain is monomeric in solution according to gel filtration chromatography and analytical ultracentrifugation (data not shown). Domain C was found to be well-suited for structural analysis using NMR methods, with sharp and disperse resonance line widths typical of a 16 kDa globular protein. NMR results show that domain C forms an α/β-structure, with regular secondary structure elements ordered in an α1-α2-α3-β1-β2-β3-α4 string along the primary sequence (Figures 3 and 4). The N-terminus of seven-turn helix α1 is completely solvent exposed and presumably forms a connection to the AB domains in the full-length PARP-1 protein. The latter two-thirds of helix α1 and all of α2 are clearly amphipathic, with one side being solvent exposed and the other side containing conserved hydrophobic residues and oriented toward the interior of the domain. Helices α1 and α2 are separated by a short three-residue kink centered at residue Ser257. Helix α3 is distinctly hydrophobic and well-conserved at its C-terminus, which is buried in the protein core. A loop connects α3 to a three-strand antiparallel β-sheet; this is the region that contains the four conserved cysteine residues. Cys295 and Cys298 are located where the loop connecting α3 with β1 reverses, with the cysteine side chains pointing toward the β-sheet. Cys311 and Cys321 are located within β2 and β3, respectively, with their side chains oriented toward Cys295 and Cys298. The C-terminal region of the domain, which includes helix α4, contacts the β-sheet and helix α3 through hydrophobic interactions among side chains. ^{15}N−^{1}H heteronuclear NOE measurements indicate that the final residues (360−373) at the C-terminus of domain C are flexible in solution, while other regions of domain C are relatively well ordered. Figure 4A shows an ensemble of the 16 lowest-energy structures. The motif containing the four conserved cysteine residues is quite well defined by the NMR data, with a backbone rmsd of only 0.49 Å when a superposition is performed using residues 291−332. Visualized in a ribbon diagram (Figure 4B), domain C appears to be segregated into distinct helical and β-sheet regions. However, the interface between the helical and β-sheet regions is populated with conserved hydrophobic residues (including Phe289, Leu292, Phe304, Trp333, Ile356, and Phe357) so that domain C is best described as being a single globular domain, rather than two subdomains connected by a linker.

Domain C Contains a Metal-Binding Motif. The four conserved cysteine residues of domain C are located close together in the three-dimensional structure, with their side chains favorably oriented so that they can bind a zinc atom. When domain C was purified from cells grown in LB broth, zinc was found to be present in the protein in an approximately 1:1 molar ratio, determined by ICP-MS, while the amounts of other metals including cobalt and copper were negligible. Removal of zinc by treatment with urea and the chelating agent 1,10-phenanthroline in the presence of DTT, followed by a return to NMR buffer, resulted in a ^{1}H NMR spectrum with chemical shifts typical of a random coil structure. Refolding of this apoprotein could be induced by the addition of zinc sulfate, as indicated by the return of the dispersed ^{1}H NMR chemical shifts typical of folded domain C. Efforts aimed at purifying a domain C mutant with Cys298 changed to alanine were unsuccessful; this mutation resulted in a low level of expression and a MBP fusion protein that was resistant to TEV protease digestion. These observations suggest that the bound zinc atom provides a critical stabilizing element and is required for the proper folding of domain C.

Interestingly, it was possible to prepare a cobalt form of domain C by growing the *E. coli* expression cells in M9 defined medium containing a 10-fold excess of cobalt (270 μg of Co/L vs 27 μg of Zn/L). Protein purified from cells grown in this cobalt-rich medium was blue in color and had a ^{1}H NMR spectrum containing several peaks shifted 20 ppm or more outside of the usual ^{1}H chemical shift range, which is typical for a protein containing a cobalt paramagnetic center. ICP-MS analysis of the purified protein revealed the presence of both cobalt and zinc in an ∼6:1 ratio. The UV−visible spectrum of the cobalt form of domain C (Figure 5) shows an intense absorption band in the near-UV region at 341 nm, which is indicative of S → Co(II) ligand to metal charge transfer (LMCT) transition. Additional bands in the 600−750 nm range are due to Co^{2+} electronic transitions from $^{4}A_2$ to ^{4T1}(P) states, and the estimated extinction coefficient at 697 nm (ϵ > 400 M^{-1} cm^{-1}) is strongly suggestive of a tetrahedral or distorted tetrahedral coordination geometry (*36*). The cobalt form of domain C was found to be relatively unstable, with a tendency to precipitate after collection of NMR data for several hours at 25 °C. In contrast, the zinc form of the protein was stable in solution for several weeks. Although the "correct" metal for domain C can only be verified by analysis of the wild-type protein from a natural (human) source, results of this work suggest that zinc is the most likely candidate, with cobalt being able to serve as a less stable substitute.

Domain C Is Essential for PARP-1 Activity. To investigate whether domain C is required for PARP-1 activity, a truncated PARP-1 module ABDEF, having domain C deleted, was constructed and purified as a single polypeptide. In the process of forming polymers of ADP-ribose, the PARP-1 enzyme catalyzes the cleavage of NAD^+ to generate free nicotinamide. The activities of PARP-1 and the truncation mutant can therefore be analyzed using NMR spectroscopy to monitor the pool of free NAD^+ as it is consumed and nicotinamide that is produced. Accordingly, the NAD^+ hydrolase activity of ABDEF was measured using this NMR-based assay (Figure 6A). No detectable nicotinamide was

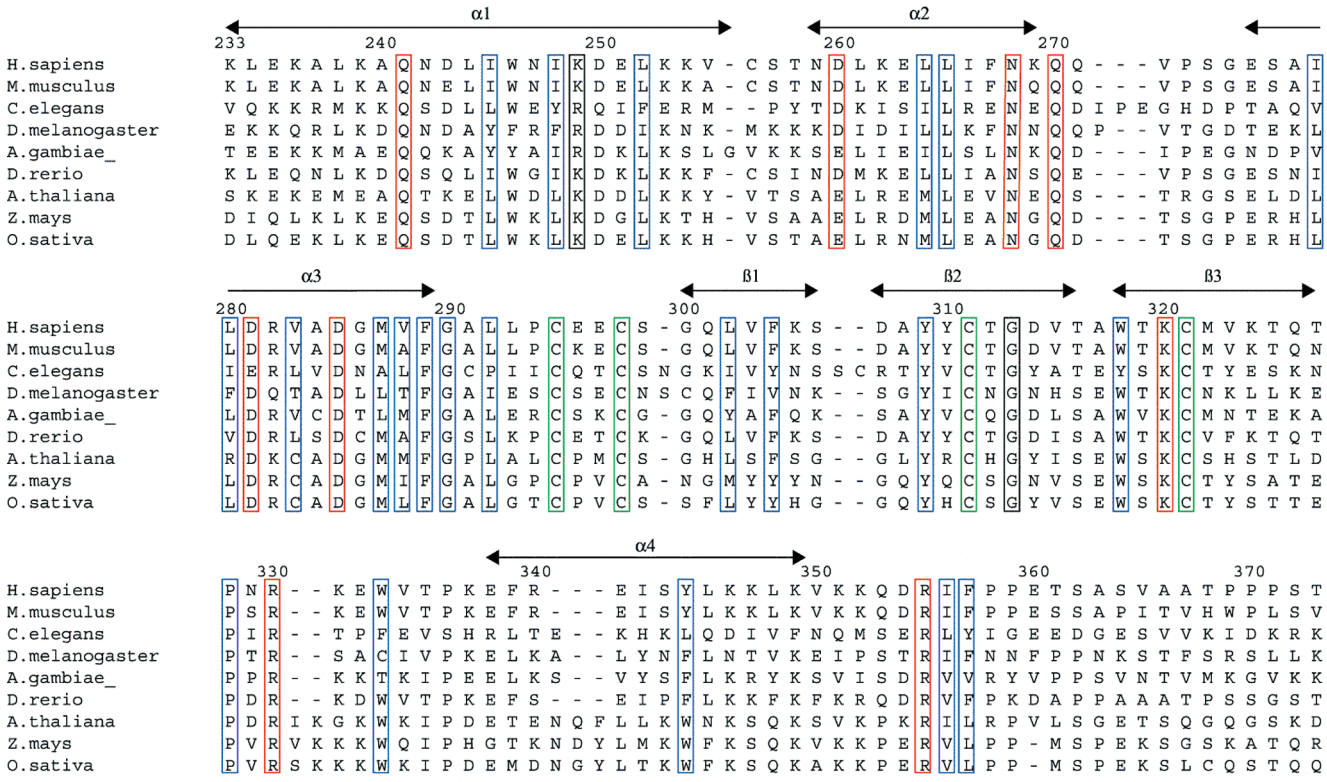

FIGURE 3: Amino acid sequence alignment of domain C of PARP-1 from nine diverse species of eukaryotes, showing the extent of the helices and strands. The four conserved cysteine residues that coordinate the zinc atom are boxed in green. Hydrophobic and glycine residues that are well-conserved and located in structurally important positions within domain C are boxed in blue; the conservation of these amino acids indicates that domain C within these diverse forms of PARP-1 is similar in structure. Conserved hydrophilic amino acids that are located on the surface of the domain are boxed in red. Two amino acids where mutations have been associated with loss of function (K249 and G313) are boxed in black and discussed in the text. Sequences are shown for *Homo sapiens*, mouse (*Mus musculus*), nematode (*Caenorhabditis elagans*), fruit fly (*Drosophila melanogaster*), mosquito (*Anopheles gambiae*), zebrafish (*Danio rerio*), and the plant species *Arabidopsis thaliana*, *Zea mays*, and *Oryza sativa*. Residues are numbered consistent with human PARP-1.

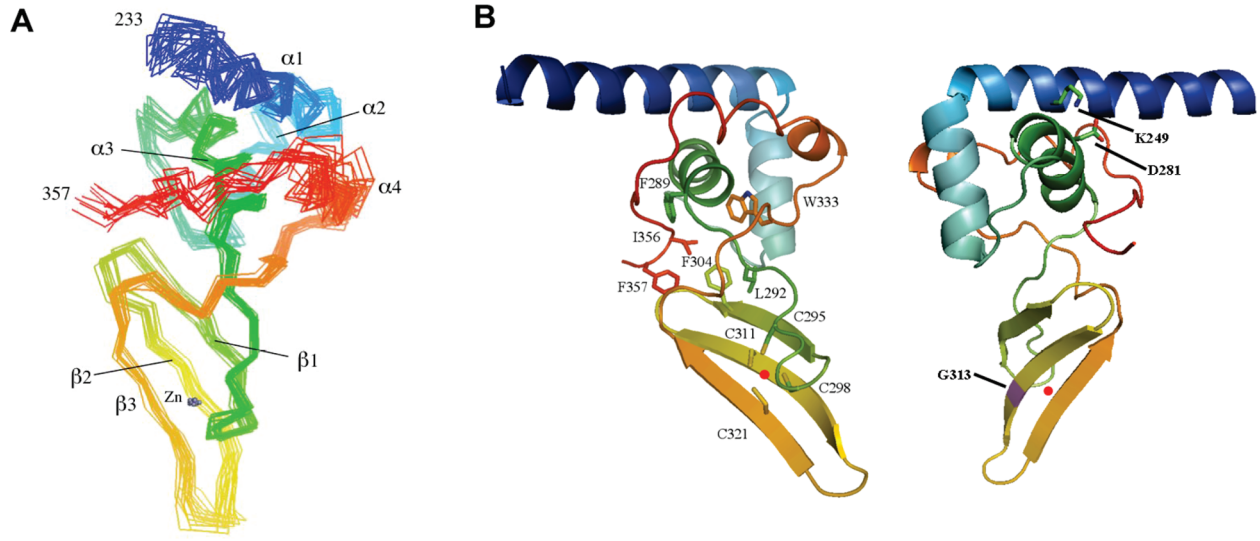

FIGURE 4: Solution structure of human PARP-1 domain C (residues 233−357). (A) Superposition of the backbones of 16 low-energy structures of domain C, color-ramped from blue (residue 233) to red (residue 357). The 16 models represent the full range of structures that are consistent with the NMR-derived constraints and reasonable molecular geometry. (B) Ribbon diagrams showing the structure of domain C, created using PyMOL (http://www.pymol.org). The location of the zinc atom is indicated by a small red sphere. The left panel shows the side chains of the four cysteines that coordinate the zinc atom and some of the conserved hydrophobic residues at the hydrophobic interface between the helical and β-sheet regions shown using sticks; the right panel shows a ribbon diagram showing a different view of domain C, indicating the locations of two amino acids where mutations have been associated with loss of function (K249 and G313), and D281, which presumably forms a salt bridge with K249.

produced after 16 h in a mixture containing 10 μM ABDEF domains of PARP-1, 15 μM nicked DNA, 10 mM $MgCl_2$, and 1 mM NAD^+, but lacking domain C (Figure 6A, right panel). Interestingly, however, when 20 μM domain C was added to this same mixture, NMR spectra showed that free nicotinamide was produced, until the pool of available NAD^+

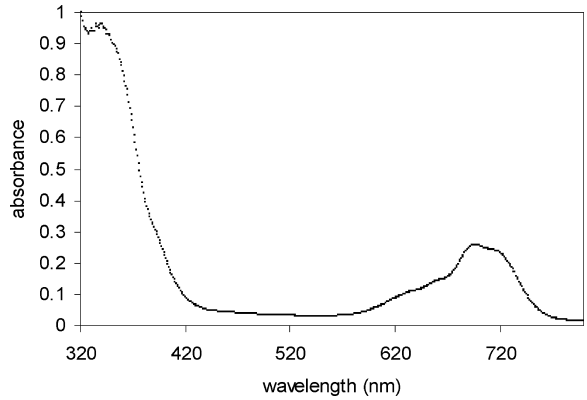

FIGURE 5: Absorption spectrum of domain C purified from cobalt-rich M9 medium, which results in a mixture of Co^{2+}-bound domain C and Zn^{2+}-bound domain C in a ratio of ~6:1. The protein concentration was 0.4 mM in HEPES buffer [20 mM HEPES buffer (pH 7.5), 300 mM NaCl, 10 mM imidazole, 10% glycerol, and 1 mM β-mercaptoethanol].

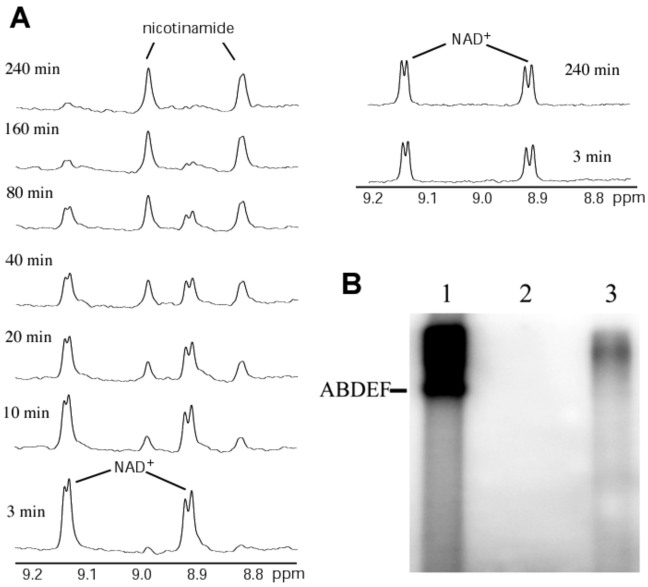

FIGURE 6: Domain C is important for PARP-1 activity. (A) Domain C is required for NAD^+ hydrolase activity. The left panel shows ^1H NMR spectra showing the consumption of NAD^+ and production of free nicotinamide in a mixture containing 10 μM ABDEF domains, 15 μM nicked DNA, 10 mM $MgCl_2$, 1 mM NAD^+, and 20 μM domain C. The initial reaction rate is 0.03 s^{-1}. The right panel shows ^1H NMR spectra of the same mixture, except domain C is not present. (B) SDS−PAGE showing the formation of poly(ADP-ribose) catalyzed by PARP-1 domains ABDEF in the presence (lane 1) or absence (lane 3) of domain C, with [α-^{32}P]NAD^+ as the substrate. The signal was detected by autoradiography. Lane 2 shows the reaction mixture without domains ABDEF, which serves as a negative control.

was almost completely depleted as observed in the NMR spectra (Figure 6A, left panel). It is important to note that domain C alone is incapable of hydrolyzing NAD^+. This NMR-based assay provides strong evidence that domain C plays an important role in the regulation of PARP-1 activity.

The ADP-ribose polymerase activity of ABDEF was further examined by monitoring the production of PAR. The assay was performed by incubation of 1 μM ABDEF, 5 μM nicked DNA, and 5 μM [α-^{32}P]NAD^+ for 30 min at room temperature. The ADP-ribosylated products were visualized by autoradiography. As shown in Figure 6B, only trace amounts of PAR-labeled products were produced when only ABDEF was present in the reaction mixture. In contrast, addition of 5 μM domain C to the same reaction mixture dramatically enhances PAR formation, underscoring the importance of domain C for PARP-1 activity. In both cases, the ADP-ribosylated products migrated as smears at high molecular masses on a SDS−PAGE gel. It is important to note that addition of domain C had little effect on the basal activity of domains ABDEF in the absence of DNA (data not shown). Thus, domain C is clearly a crucial component in DNA-dependent PARP-1 activation.

Domain C and DNA. The DNA binding function of PARP-1 has previously been attributed to the zinc-finger motifs of domain A. However, the identification of the novel zinc-binding motif in domain C raises the question of whether domain C is involved in the PARP-1−DNA interaction, since proteins containing zinc-binding motifs are commonly associated with DNA. To answer this question, NMR methods were used to detect any putative interactions between domain C and DNA. Our results showed that the ^1H 1D and $^{15}N-^1H$ correlated 2D NMR spectra of domain C were unchanged upon the addition of an excess of an 18 bp double-stranded DNA with free DNA ends, a structure element known to preferentially bind to cloned PARP-1 in vitro (*37*). Conversely, addition of domain C did not induce any change in the ^1H NMR spectrum of the double-stranded DNA. Negative results were also obtained when a 44-mer oligonucleotide with a dumbbell secondary structure that has previously been used as a model for nicked DNA (*38*) was used as a potential binding partner. In addition, a dot blotting assay using a biotin−streptavidin system failed to detect any interaction between domain C and calf thymus DNA. In contrast, domains AB exhibit significant binding toward these DNA fragments in these experiments. In summary, the observations described above did not uncover any evidence that domain C binds to DNA, at least in its isolated form.

DISCUSSION

An understanding of the enzymatic complicity of PARP-1 requires a detailed knowledge of the structure and function of each domain. The structural information provided by this work defines the locations of the amino acids within domain C and permits us to gain some insight into why particular amino acids are conserved or important for function. Of particular interest is Lys249, since mutations of this residue have previously been shown to lead to a loss of function (*23*). Lys249 is located adjacent to Asp281, in a position that suggests a salt bridge between these two conserved and oppositely charged residues, located in helices α1 and α3, respectively. Lys249 may therefore be important for maintaining the proper juxtaposition between α1 and α3. Other conserved amino acids form the hydrophobic core of domain C (and are boxed in blue in Figure 3); these are presumably important for protein stability. The strong conservation of hydrophobic amino acids in structurally important locations, as well as the conservation of the four zinc-binding cysteines, indicates that the overall fold of domain C is maintained among the diverse forms of PARP-1, from humans to plants (Figure 3). In addition to the conserved hydrophobic core residues, domain C also contains several conserved hydrophilic amino acids located on the surface, which could potentially mediate intermolecular interactions (with enzyme

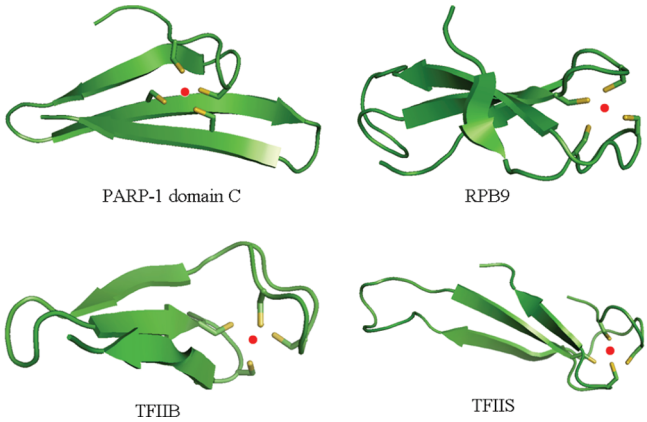

FIGURE 7: Ribbon diagrams comparing the zinc-binding motif of domain C of PARP-1 with RNA polymerase II subunit 9 (RPB9) from *Thermococcus celer*, the N-terminal domain of transcriptional elongation factor TFIIB from *Pyrococcus furiosus*, and the nucleic acid binding domain of human transcriptional elongation factor TFIIS, created by PyMOL using coordinates from PDB entries 1QYP, 1PFT, and 1TFI, respectively. The side chains of cysteines that coordinate to zinc are shown with sticks, and the zinc ion in each structure is shown as a red sphere.

substrate or product) or intramolecular interactions with other PARP domains. The most variable parts of the domain C sequence occur in the loop connecting strand β3 with helix α4, where the plant enzymes appear to have a short (two or three residue) insertion, and in the flexible C-terminal segment after residue 357 (Figure 3). The helices within domain C are not arranged in a canonical helix−turn−helix motif, as previously predicted (*20, 21*).

A comparison of domain C with the structures in the zinc-finger database was performed. The term "zinc finger" is not restricted to DNA binding proteins with fingerlike motifs closely related to TFIIIA but was broadened to include any compact domain stabilized by zinc. On the basis of the spatial arrangement of secondary structural elements in the vicinity of the zinc-binding sites, the zinc-finger structures can be divided into eight different folds (*39*). The zinc-binding motif of domain C having a sequence of $CX_2CX_{12}CX_9C$ is distinct in terms of its inter-cysteine spacing and structural details. It is structurally most similar to the zinc-ribbon fold, but with its own unique features (Figure 7). The core structure of a typical zinc ribbon is composed of two β-hairpins that form two structurally similar zinc-binding subsites, with additional β-strands in the proximity forming hydrogen bonds with one of the hairpins. In some cases, one or both pairs of the zinc-binding ligands are from a nearby loop instead of the hairpin, such as in RPB9 (*40*), TFIIB (*41*), and TFIIS (*42*) (Figure 7). The zinc-binding motif in domain C contains a three-stranded antiparallel β-sheet, with the first pair of zinc ligands located in the loop running over the top of the sheet. The other pair of zinc ligands is centrally located within β-strands, a result of a long (nine-amino acid) insertion between the third and fourth cysteines. Within this insertion, it was reported earlier that a mutant of G313E abolished PARP-1 activity, which may now be attributed to the alteration in the structure near the metal-binding motif due to the change in the side chain.

Comparing the recently reported crystal structure of domain C of human PARP-1 (*26*) and the solution structure showed that both are similar in the descriptions of helices α1−α3, as well as the antiparallel β-sheet that forms the zinc-binding motif, but differ in the descriptions of the C-terminal region of the domain (Figure 8). In the crystal structure, the residues nearest the C-terminus make extended contacts with another copy of the domain to form a symmetric dimer; in contrast, the domain is monomeric in solution. The differences between the structures may be a result of the solution conditions required for crystal growth or the intermolecular contacts induced by crystal packing or due to the fact that the construct used in determining the solution structure contained 17 fewer amino acids at its N-terminus and seven additional amino acids at its C-terminus, compared to the construct used for the crystal structure. Although full-length PARP-1 is believed to be dimeric during catalysis on the basis of kinetic analysis (*43*), whether PARP-1 exists as a dimer in the absence of DNA has not yet been fully defined. Clearly, additional biophysical studies are needed to develop a more complete understanding of how this multidomain protein is assembled in three dimensions.

The activity assays in this work show that domains ABDEF exhibit only a low (basal) enzymatic activity, with the activity being greatly increased upon the addition of domain C; this suggests an important role for domain C in proper PARP-1 function. However, the molecular mechanisms underlying the requirement of domain C for full PARP-1 activity remain obscure. The location of domain C

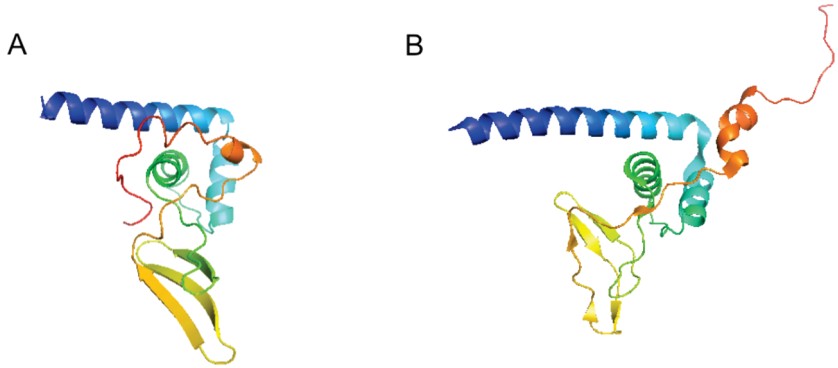

FIGURE 8: Comparison of the solution structure (A) and crystal structure (B) of domain C of human PARP-1. The structures are similar in helices α1−α3 and the zinc-binding motif but differ in the arrangement of helix α4 and the C-terminal region of the domain. In solution, the domain is a monomer, while in the crystal structure, the C-terminal residues (colored red) contact another copy of the domain to form a symmetric dimer (*26*). The solution structure contains eight fewer amino acids at its N-terminus and 2 fewer amino acids at its C-terminus compared to the crystal structure. The models are derived from PDB entries 2JVN and 2RIQ, respectively.

in the primary sequence of PARP-1, between the zinc-finger DNA-binding domains at the N-terminus of the protein and the catalytic domain at the C-terminus (Figure 1B), suggests that the functional role of domain C may be in relaying the signal of "PARP-1 binding to DNA" to the catalytic domain, perhaps by inducing a rearrangement in the protein, giving rise to a new conformation that is more favorable for catalysis. It is noteworthy that Sir2-Af1, a histone deacetylase which produces nicotinamide and *O*-acetyl-ADP-ribose with the consumption of NAD^+, also contains a zinc-ribbon motif (*44*). Although the zinc-ribbon motif in Sir2-Af1 extends out from the main body of the structure and is far from the NAD^+-binding pocket, it contributes to the maintenance of a large cleft which is proposed to be the protein substrate binding site.

Likewise, domain C might also help to stabilize a conformation that allows the docking of the automodification domain or other PARP-1 substrates near the enzyme's active site. Alternatively, domain C may facilitate PARP-1 activity through other mechanisms such as product stabilization. For example, amphipathic α1 could form electrostatic contacts with the nascent PAR chains, thus ensuring a processive reaction. Another candidate to play this role is the zinc-ribbon motif. Although zinc fingers are best recognized as sequence-specific DNA-binding motifs, they have evolved as versatile structural scaffolds that also allow RNA or protein binding. It therefore would not be surprising if the zinc ribbon in domain C could interact with the negatively charged PAR. Even though domain C does not bind to DNA by itself, the possibility remains that it might cooperate with the other two PARP-1 zinc fingers to achieve effective and functional DNA binding. Clearly, more detailed analysis needs to be carried out to fully elucidate the role of domain C in PARP-1 catalysis.

Finally, it has been established that PARP-1 inhibitors have wide therapeutic applications in cancer and many oxidative damage-related diseases (*45, 46*). However, all the current agents under clinical development target the active site of the enzyme. While these agents show considerable promise, the issue of off-target effects is a concern due to the existence of multiple PARPs. Given the facts that domain C is important for DNA-dependent PARP-1 activation and there is no sequence homology of domain C with other known functional motifs, the structural and activity studies of domain C presented here provide a potential new avenue for the development of more selective PARP-1 inhibitors.

REFERENCES

1. Satoh, M. S., and Lindahl, T. (1992) Role of poly(ADP-ribose) formation in DNA repair. *Nature 356*, 356–358.
2. Yang, Y. G., Cortes, U., Patnaik, S., Jasin, M., and Wang, Z. Q. (2004) Ablation of PARP-1 does not interfere with the repair of DNA double-strand breaks, but compromises the reactivation of stalled replication forks. *Oncogene 23*, 3872–3882.
3. Meyer-Ficca, M. L., Meyer, R. G., Jacobson, E. L., and Jacobson, M. K. (2005) Poly(ADP-ribose) polymerases: Managing genome stability. *Int. J. Biochem. Cell Biol. 37*, 920–926.
4. Leduc, Y., Lawrence, J. J., De Murcia, G., and Poirier, G. G. (1988) Cell cycle regulation of poly(ADP-ribose) synthetase in FR3T3 cells. *Biochim. Biophys. Acta 968*, 275–282.
5. Kraus, W. L., and Lis, J. T. (2003) PARP goes transcription. *Cell 113*, 677–683.
6. Yu, S. W., Wang, H., Poitras, M. F., Coombs, C., Bowers, W. J., Federoff, H. J., Poirier, G. G., Dawson, T. M., and Dawson, V. L. (2002) Mediation of poly(ADP-ribose) polymerase-1-dependent cell death by apoptosis-inducing factor. *Science 297*, 259–263.
7. Alvarez-Gonzalez, R., and Althaus, F. R. (1989) Poly(ADP-ribose) catabolism in mammalian cells exposed to DNA-damaging agents. *Mutat. Res. 218*, 67–74.
8. Kaufmann, S. H., Desnoyers, S., Ottaviano, Y., Davidson, N. E., and Poirier, G. G. (1993) Specific proteolytic cleavage of poly-(ADP-ribose) polymerase: An early marker of chemotherapy-induced apoptosis. *Cancer Res. 53*, 3976–3985.
9. Martin, D. S., Bertino, J. R., and Koutcher, J. A. (2000) ATP depletion + pyrimidine depletion can markedly enhance cancer therapy: Fresh insight for a new approach. *Cancer Res. 60*, 6776–6783.
10. Tulin, A., and Spradling, A. (2003) Chromatin loosening by poly(ADP)-ribose polymerase (PARP) at *Drosophila* puff loci. *Science 299*, 560–562.
11. Kim, M. Y., Mauro, S., Gevry, N., Lis, J. T., and Kraus, W. L. (2004) NAD^+-dependent modulation of chromatin structure and transcription by nucleosome binding properties of PARP-1. *Cell 119*, 803–814.
12. Schreiber, V., Dantzer, F., Ame, J. C., and de Murcia, G. (2006) Poly(ADP-ribose): Novel functions for an old molecule. *Nat. Rev. Mol. Cell Biol. 7*, 517–528.
13. Kameshita, I., Matsuda, Z., Taniguchi, T., and Shizuta, Y. (1984) Poly (ADP-Ribose) synthetase. Separation and identification of three proteolytic fragments as the substrate-binding domain, the DNA-binding domain, and the automodification domain. *J. Biol. Chem. 259*, 4770–4776.
14. de Murcia, G., and Menissier de Murcia, J. (1994) Poly(ADP-ribose) polymerase: A molecular nick-sensor. *Trends Biochem. Sci. 19*, 172–176.
15. Gradwohl, G., Menissier de Murcia, J. M., Molinete, M., Simonin, F., Koken, M., Hoeijmakers, J. H., and de Murcia, G. (1990) The second zinc-finger domain of poly(ADP-ribose) polymerase determines specificity for single-stranded breaks in DNA. *Proc. Natl. Acad. Sci. U.S.A. 87*, 2990–2994.
16. Schreiber, V., Molinete, M., Boeuf, H., de Murcia, G., and Menissier-de Murcia, J. (1992) The human poly(ADP-ribose) polymerase nuclear localization signal is a bipartite element functionally separate from DNA binding and catalytic activity. *EMBO J. 11*, 3263–3269.
17. Bork, P., Hofmann, K., Bucher, P., Neuwald, A. F., Altschul, S. F., and Koonin, E. V. (1997) A superfamily of conserved domains in DNA damage-responsive cell cycle checkpoint proteins. *FASEB J. 11*, 68–76.
18. Semighini, C. P., Savoldi, M., Goldman, G. H., and Harris, S. D. (2006) Functional characterization of the putative *Aspergillus nidulans* poly(ADP-ribose) polymerase homolog PrpA. *Genetics 173*, 87–98.
19. Simonin, F., Menissier-de Murcia, J., Poch, O., Muller, S., Gradwohl, G., Molinete, M., Penning, C., Keith, G., and de Murcia, G. (1990) Expression and site-directed mutagenesis of the catalytic domain of human poly(ADP-ribose)polymerase in *Escherichia coli*. Lysine 893 is critical for activity. *J. Biol. Chem. 265*, 19249–19256.
20. Uchida, K., Morita, T., Sato, T., Ogura, T., Yamashita, R., Noguchi, S., Suzuki, H., Nyunoya, H., Miwa, M., and Sugimura, T. (1987) Nucleotide sequence of a full-length cDNA for human fibroblast poly(ADP-ribose) polymerase. *Biochem. Biophys. Res. Commun. 148*, 617–622.
21. Saito, I., Hatakeyama, K., Kido, T., Ohkubo, H., Nakanishi, S., and Ueda, K. (1990) Cloning of a full-length cDNA encoding bovine thymus poly(ADP-ribose) synthetase: Evolutionarily conserved segments and their potential functions. *Gene 90*, 249–254.
22. Sastry, S. S., Buki, K. G., and Kun, E. (1989) Binding of Adenosine Diphosphoribosyltransferase to the Termini and Internal Regions of Linear DNAs. *Biochemistry 28*, 5670–5680.
23. Trucco, C., Flatter, E., Fribourg, S., de Murcia, G., and Menissier-de Murcia, J. (1996) Mutations in the amino-terminal domain of the human poly(ADP-ribose) polymerase that affect its catalytic activity but not its DNA binding capacity. *FEBS Lett. 399*, 313–316.
24. Ruf, A., Mennissier de Murcia, J., de Murcia, G., and Schulz, G. E. (1996) Structure of the catalytic fragment of poly(AD-ribose) polymerase from chicken. *Proc. Natl. Acad. Sci. U.S.A. 93*, 7481–7485.
25. Kinoshita, T., Nakanishi, I., Warizaya, M., Iwashita, A., Kido, Y., Hattori, K., and Fujii, T. (2004) Inhibitor-induced structural change of the active site of human poly(ADP-ribose) polymerase. *FEBS Lett. 556*, 43–46.

26. Langelier, M. F., Servent, K. M., Rogers, E. E., and Pascal, J. M. (2008) A third zinc-binding domain of human poly(ADP-ribose) polymerase-1 coordinates DNA-dependent enzyme activation. *J. Biol. Chem. 283*, 4105–4114.
27. Wang, J., and Wilkinson, M. F. (2001) Deletion mutagenesis of large (12-kb) plasmids by a one-step PCR protocol. *BioTechniques 31*, 722–724.
28. Muhandiram, D. R., and Kay, L. E. (1994) Gradient-enhanced triple resonance three-dimensional NMR experiments with improved sensitivity. *J. Magn. Reson., Ser. B 103*, 203–216.
29. Grzesiek, S., and Bax, A. (1992) ^{1}H, ^{13}C, and ^{15}N NMR backbone assignments and secondary structure of human interferon-γ. *J. Magn. Reson. 96*, 432–440.
30. Kay, L. E. (1993) Pulsed-field gradient-enhanced three-dimensional NMR experiment for correlating $^{13}C'$, $^{13}C'$, and $^{1}H'$ chemical shifts in uniformly ^{13}C-labeled proteins dissolved in H_2O. *J. Am. Chem. Soc. 115*, 2055–2057.
31. Kay, L. E., Xu, G. Y., Singer, A. U., Muhandiram, D. R., and Forman-Kay, J. D. (1993) A gradient-enhanced HCCH-TOCSY experiment for recording side-chain ^{1}H and ^{13}C correlations in H_2O samples of proteins. *J. Magn. Reson., Ser. B 101*, 333–337.
32. Delaglio, F., Grzesiek, S., Vuister, G. W., Zhu, G., Pfeifer, J., and Bax, A. (1995) NMRPipe: A multidimensional spectral processing system based on UNIX pipes. *J. Biomol. NMR 6*, 277–293.
33. Wishart, D. S., Bigam, C. G., Yao, J., Abildgaard, F., Dyson, H. J., Oldfield, E., Markley, J. L., and Sykes, B. D. (1995) ^{1}H, ^{13}C and ^{15}N chemical shift referencing in biomolecular NMR. *J. Biomol. NMR 6*, 135–140.
34. Brunger, A. T., Adams, P. D., Clore, G. M., DeLano, W. L., Gros, P., Grosse-Kunstleve, R. W., Jiang, J. S., Kuszewski, J., Nilges, M., Pannu, N. S., et al. (1998) Crystallography & NMR system: A new software suite for macromolecular structure determination. *Acta Crystallogr. D54*, 905–921.
35. Berjanskii, M. V., Neal, S., and Wishart, D. S. (2006) PREDITOR: A web server for predicting protein torsion angle restraints. *Nucleic Acids Res. 34*, W63–W69.
36. Krizek, B. A., Merkle, D. L., and Berg, J. M. (1993) Ligand variation and metal-ion binding specificity in zinc finger peptides. *Inorg. Chem. 32*, 937–940.
37. Lonskaya, I., Potaman, V. N., Shlyakhtenko, L. S., Oussatcheva, E. A., Lyubchenko, Y. L., and Soldatenkov, V. A. (2005) Regulation of Poly(ADP-ribose) Polymerase-1 by DNA Structure-specific Binding. *J. Biol. Chem. 280*, 17076–17083.
38. Kulczyk, A. W., Yang, J. C., and Neuhaus, D. (2004) Solution structure and DNA binding of the zinc-finger domain from DNA ligase IIIα. *J. Mol. Biol. 341*, 723–738.
39. Krishna, S. S., Majumdar, I., and Grishin, N. V. (2003) Structural classification of zinc fingers: Survey and summary. *Nucleic Acids Res. 31*, 532–550.
40. Wang, B., Jones, D. N., Kaine, B. P., and Weiss, M. A. (1998) High-resolution structure of an archaeal zinc ribbon defines a general architectural motif in eukaryotic RNA polymerases. *Structure 6*, 555–569.
41. Zhu, W., Zeng, Q., Colangelo, C. M., Lewis, M., Summers, M. F., and Scott, R. A. (1996) The N-terminal domain of TFIIB from *Pyrococcus furiosus* forms a zinc ribbon. *Nat. Struct. Biol. 3*, 122–124.
42. Qian, X., Gozani, S. N., Yoon, H., Jeon, C. J., Agarwal, K., and Weiss, M. A. (1993) Novel zinc finger motif in the basal transcriptional machinery: Three-dimensional NMR studies of the nucleic acid binding domain of transcriptional elongation factor TFIIS. *Biochemistry 32*, 9944–9959.
43. Mendoza-Alvarez, H., and Alvarez-Gonzalez, R. (1993) Poly(ADP-ribose) polymerase is a catalytic dimer and the automodification reaction is intermolecular. *J. Biol. Chem. 268*, 22575–22580.
44. Min, J., Landry, J., Sternglanz, R., and Xu, R. M. (2001) Crystal structure of a SIR2 homolog-NAD complex. *Cell 105*, 269–279.
45. Zaremba, T., and Curtin, N. J. (2007) PARP inhibitor development for systemic cancer targeting. *Anticancer Agents Med. Chem. 7*, 515–523.
46. Virag, L., and Szabo, C. (2002) The therapeutic potential of poly(ADP-ribose) polymerase inhibitors. *Pharmacol. Rev. 54*, 375–429.

BI800018A